The eletrochemical evaluation of the influence of titanium and molybdenum alloy elements in 13cr supermartensitic and 13cr martensitic stainless steels in different concentrations of chloride solutions

Josemar C. Josemar[a], Jefferson O. Jefferson[b], José P. José[c], Alysson. B[d]

Abstract

The corrosion susceptibility in 13Cr martensitic stainless steel (MSS) and 13Cr supermartensitic stainless steel (SMSS) was investigated by potentiodynamic polarization and electrochemical impedance spectroscopy (EIS). This study was conducted to analyze the susceptibility of pitting corrosion at different concentrations of chloride solution (5%, 10% and 20%) and the influence of molybdenum (Mo) and titanium (Ti) as alloy elements in the steel. The polarization curves showed that the passive film formed is affected by increasing chloride concentration. Nyquist diagrams were determined by EIS to characterize the resistance of the passive layer. There was a greater resistance to pitting corrosion of super martensitic steels than the conventional martensitic steels. This result can be attributed to presence of alloy elements, such as, Mo and Ti which promotes the possible formation of dual passive layer, although studies report that the titanium in the presence of nitrogen and carbon favors the formation of precipitates, which may cause intergranular corrosion.

Keyword: 13Cr and S13Cr, supemartensitic steels, corrosion, chloride solution, polarization, Impedance spectroscopy.

Introdution

Due to its excellent combination properties, martensitic stainless steel and supermartensitic has increasingly attracted interest in the industries of oil and gas offshore. [*4*]. When comparing the SMSS steels have higher strength, hardness, corrosion resistance and weldability compared to steels MSS. These properties can vary depending on the seasons and tempered balance and chemical composition. However improper heat treatment should cause

---

[a] Engenheiro Mecânico – Universidade Federal de São João Del Rei
[b] Mestre, Engenheiro Mecânico - Centro de Pesquisas e Desenvolvimento Leopoldo Américo Miguez de Mello (Cenpes)
[c] Doutor, Engenheiro Metalurgista – Universidade Federal do Rio de Janeiro
[d] Doutor, Engenheiro Mecânico – Universidade Federal de São João Del Rei

significant changes in the microstructure and serious reductions in the values of mechanical properties. [*15*]

Corrosion of stainless steels has been studied extensively with the role of passive film, a nano film rich in chromium that can inhibit steel corrosion. Furthermore, promotion of the formation of a passive film on the pit chloride ions and properties of alloy elements such as Cr, Ni, Mo to inhibit pitting. [*16*]. Special alloys that retard corrosion can be formed on the surface. Titanium and its alloys have good corrosion resistance in acid and humid conditions even at high positive overpotentials.[*6*]

Pitting corrosion comprises two processes: pit nucleation and pit growth. Some authors have considered that pit initiation is attributed to the breakdown of the passivel film layer caused by ranbom fluctuation at local sites. After pit nucleation occurs, the pit can repassivate immediately or grow and them repassivate. In general, this process is regarded as metastable pitting. If a metastable pit can grow indefinitely, it becomes a stable pit. [*19*]

In this work the Cr13 SMSS and MSS has been studied and the effect of concentrations of chloride, influence of the Mo and Ti in the stainless steel alloys and pitting formation.

Experimental Procedure

Chemical Evaluation

Four samples of stainless steel were tested in order to evaluate the corrosion resistance, being two supermartensitics 13Cr (S13Cr) and two matensitics 13Cr (13Cr). The chemical composition of the steels are presented in the table 1. Then, the chemical composition was examined according to the Standard ISO 13680 Martensitic / UNS number S41426, ISO 15156-3:2009 420 M and Schaeffler diagram Figure 6. According to the Schaeffler diagram, it is possible to characterize the microstructure of a determined material based on chromium equivalent and nickel equivalent to CRA alloys [*13*]. The reading of the diagram is given by the chemical composition, Table 1, together with the aid of a mathematical formula, Table 6, which obtains the values of nickel equivalent and chromium equivalent, Table 7 and 8.

The microstructure characterization of the specimens was performed by conventional metallographic chemical attack with Villela reagent (5 ml of HCl + 100 ml of C2H5OH + 1g picric acid), followed by observation under optical microscope and scanning electron microscope.

Electrochemical measurements

The potentiodynamic polarization experiments were performed in different naturally aerated solutions, being 5%, 10% and 20% of sodium chloride. The impedance electrochemical test was only analyzed in the aerated solution with 5% of NaCl.

The tests were carried out using the method of potentiodynamic polarization in a conventional electrochemical cell with three electrodes, being a platinum auxiliary electrode, a reference of saturated calomel electrode (SCE) and a working electrode. The working electrodes were prepared with 24 hours prior to the electrochemical tests.

The potentiodynamic polarization curves were obtained with the aid of a potentiostat AUTOLAB PGSTAT101 at a scan rate of 0.001 V/s, according to standard ASTM G5 - 94.

The impedance tests was accomplished on OCP potential, 50mV above OCP potential, 100mV above OCP potential and 150mV above OCP potential. On the impedance curves are shown the Z’ real polarization resistance and Z’’ imaginary polarization resistance.

Before of the all electrochemical experiment the samples were stabilized 1 hours on solution test in potential open circuit (OCP).

Results and Discussion

Chemical composition

The chemical compositions were analyzed and compared with various standards, showing the standard ISO13680 / UNS number S41426 compatible with the chemical composition of supermartensitic steel 13Cr (samples 1-S13Cr and sample 2-S13Cr). For martensitic steels (sample 3-13Cr and sample 4-13Cr), the standard ISO 15156-3:2009 / name 420 M presented compatibility.

In general, all the samples show a typical microstructure of ferrite and martensite.

Sample 1-S13Cr showed TiN precipitates in the form of irregular cubic crystals throughout the sample due to addition of Ti in the composition of stainless steel.

Although the Ti promotes the formation of a passive double layer in order to increase the corrosion resistance of the steel, the same has a great affinity with C and N which can generate the formation of precipitates of TiC and TiN. [*9*].

The formation of the passivating film is due to the presence of passivation elements, as Cr_2O_3. The addition of Mo also improves the corrosion pitting resistance of the stainless steel. When included as an alloying element, Mo is incorporated into the passive film, producing oxides with different oxidation states. The most common corrosion product incorporated into the Cr oxide layer is $MoO^{2-}{}_{4,}$ which is extremely stable and fixes this layer. [*17*]

Schaeffler diagram

The chemical composition of the all samples was interpreted according to the Schaeffler diagram, which obtained a microstructure of martensite and ferrite. The microscopy of the samples presented a structure very similar to that described by Schaeffler diagram, showing a martensitic phase and a ferritic shown in Figures 2, 3, 4, 5.

Potentiodynamic Polarizations

The Figures 11, 12, 13 and 14 shows the anodic polarization curves of martensitic and supermartensitic stainless steels in different concentrations of NaCl solutions, such as 5, 10 and 20% NaCl, naturally aerated.

The supermartensítics steels (1-S13Cr and 2-S13Cr) presented a domain of passivation. The domain of passivation showed difference between the corrosion potential and the potential for pitte. It can be seen that with increasing concentration of sodium chloride reduces the domain of passivation of the steels. It´s probably occurred because of the ions a chloride penetrates into the film and attack the steel.

The Tables 9, 10 and 11 show the pitting potential, passivation domain, current density on 50 and 100mV above corrosion potential.

The martensitic steels (1-13Cr and 2-13Cr) showed active dissolution process in all solutions tested. It were not observed any passivation process on the martensitc steels tested in solution with 5%, 10% and 20% of NaCl.

Therefore, the steels that presented the best resistance to pitting corrosion were 1-S13Cr and 2-S13Cr. In this case, they showed highest pitting potential and lowest current density at the pitting potential.

Studies have reported that the effect of Mo can be observed with the increase of the passivation interval and with a reduction current density. The use of Mo and Ti in the alloy promotes formation of a second passive layer making the material more resistant to corrosion. According to the mechanism of formation of dual passive layer through utilization of molybdenum as an alloying element, it is possible to deduce that the Fe ions was deposited on the sample surface in the form of $Fe_2(MoO_4)_3$. [*15*, *7*, *1*, *6*].

EIS measurements

Fig. 15 and 16 shows typical Nyquist impedance plots referring to the S13Cr steels immersed in 5% chloride sodium solution. The Nyquist impedance was tested in different potentials, being her on OCP potential, 50mV above OCP, 150mV above OCP, to evaluate the influence of electric potential on the characteristics along of the passive film.

Fig. 17 and 18 show Nyqusit impedance plots referring to the 13Cr steels immersed in 5% chloride sodium solution. The Nyquist impedance was tested in different potentials on OCP, 50mV above OCP, 100mV above OCP. The last potential tested on impedance was 100mV, because when tested this steel above 100mV, this steel shown formation pits.

The polarization resistance, Rp, is commonly used as a measure of the resistance of a metal to the corrosion damage. A high value of Rp is associated with a high corrosion prevention capability; a low value of Rp indicates potential high corrosion activity [*12*].

The experiment showed a high impedance value of Rp for super martensitic steels, Table 12, these results suggest a high degree of protection of the passive film formed. It can be observed an increase in protection is increased as the applied potential.

For martensitic steels has been a low Rp, showing a less passive film in relation to super martensitic steel. This difference between Rp super martensitic steels and martensitic can be explained by the presence of Mo, Ni, Nb in super martensitic steels [*8*].

In supermartensitic alloys, the Cr and Ni ratio equivalents promote the formation of a martensite and retained austenite microstructure. The presence of retained austenite is beneficial to supermartensitic alloys because it promotes the dissolution of Mo and Cr carbonitrides, increasing the content of these elements dissolved in the matrix [*1*].

EDS measurements

Through the EDS test was possible clearly identify the Ti precipitates as shown in Figure 19-A and 19-B. These precipitates were observed only in sample 1 because it was the only one to present relevant Ti concentrations. In Figure 20-A and 20-B was possible to identify the presence of Nitrogen (N) precipitates, which leads us to conclude that these precipitates are not only Ti, but possibly TiN.

When Ti precipitates are formed, occurs the formation of a precipitate of un-reacted Cr around the Ti. Eventually, the segregation of un-reacted Cr cause depletion of Cr adjacent to segregation thereby causing intergranular corrosion [*9*].

This can be confirmed in Figure 19-A and 19-B, where figure 19-B shows the highest concentration of TiN precipitates and also a higher concentration of pitting due to the depletion of Cr caused by the TiN formation and the generation of precipitates un-reacted Cr . Finally, in Figure 21-A and 21-B the chemical composition of the structure can be seen by means of ESD test.

Pit corrosion

The martensitic steels exhibited dissolution active, there is not passive region, the impedance results showed a reduction in linear polarization resistance is increased as the applied potential.

On the table 12 that the real resistence of the supermartensitic steel bigger than martensitic steel. It occurred because the martesitic steel do not presented passivation process, as verified with super martensitc steels.

The observed morphology of the figures 6, 7, 8 and 9, can be characterized due to the penetration mechanisms, which are caused by increased concentration of cations within the pit generating their growth.

This phenomenon is due to reduction in diffusion of metal cations in the mouth of the pit to the active dissolution, thus creating a possible repassivation this area. The deeper pit area, however, is still in active dissolution maintaining its growth [*14*].

According to Yin [*19*] corrosion pit is related to the nucleation process and growth of the pit. It is believed that due to local breakdown of passive film which results in rapid dissolution of exposed metal in the presence of aggressive ions such as sodium chloride.

The pitting corrosion occurs since the anode area is located at points where passivity destruction had and as these areas are too small in relation to the cathode area, there will be accelerated corrosion at those points.

Conclusions

The S13Cr steels had a better corrosion performance when compared with the 13Cr presenting domain of passivation at all concentrations chloride . The presence of Mo in the chemical composition of S13Cr assigns an improvement in corrosion resistance due to formation of a passive double layer. The super 13Cr steels showed cleavage activates possessing no passivation process.

The addition of the Ti alloy can assist in pitting corrosion, in the presence of N, TiN generating and enhancing intergranular corrosion.

Acknowledgement

This research was financially supported by UFSJ, CAPES, FAPEMIG and CNPQ.

Bibliography

[1]. ANSELMO, N., “Corrosion behavior of supermartensitic stainless steel in aerated and CO2-saturated synthetic seawater. Materials Science and Engineering.” A 428 (2006) 73–79, São Paulo.

[2]. ASM Handbook, Volume 1 - 13, 2004.

[3]. ASTM-G5 - 94, “Standard Test Method for Making Potentiostatic and Potentiodynamic Anodic Polarization Measurements”, American Society for Testing Materials, 1969.

[4]. BOJACK, A. “In-situ determination of austenite and martensite formation in 13cr6Ni2Mo supermartensitic stainless steel.” Materiaks Characterization 71 (2012) 77-86.

[5]. CALLISTER, W. D. Jr., " Science and Engineering of Materials: An Introduction." 7th ed. Rio e Janeiro, Technical and Scientific Books Publisher, 2008.

[6]. FENG, K., “Improved corrosion resistence of stainless steel 316L by Ti ion implantation.” Materials Letters 60 (2012) 450-452.

[7]. FENG, Z., “Passivity of 316L stainless steel in borate buffer solution studied by Mott-Schottky analysis, atomic absorption spectrometry and X-ray photoelectron spectroscopy.” Corrosion Science 52 (2010) 3646-3653.

[8]. H. Amaya, “Effect of Cr and Mo on corrosion resistance of super 13Cr martensitic stainless steel in CO2 environment”. Corrosion 98, Paper #113, 1998.

[9]. KIM, J. K.,“Effect of chromium content on intergranular corrosion and precipitation of Ti-stabilized ferritic stainless steels.” Corrosion Science 52 (2010) 1847-1852.

[10]. NACE RP- 09084, Recommended Practice “Sour Service Limits of 13% Cr and Super 13% Cr Stainless Steels for Octg: Effect of Environmental Factors” Corrosion Department, France.

[11]. NACE - 00152, Recommended Practice “Corrosion Performance of Stainless Steels” SINTEF Materials Technology, Norway.

[12]. MOREIRA, R. M., “The effects of temperature and hydrodynamics on the CO2 corrosion of 13Cr and 13Cr5Ni2Mo stainless steels in the presence of free acetic acid.” Corrosion Science 46 (2004) 2987-3003, Rio de Janeiro.

[13]. OLSON, D. L., “Prediction of Austenitic Weld Metal Microstructure and Properties.” Welding Research Supplement.

[14]. PICON, C. A., “Study of pitting corrosion mechanism of supermartensitic stainless steels microalloyed with Nb and Ti in sea water.” Rev. Esc. Minas Jan./Mar. 2010 vol.63 no.1, Ouro Preto.

[15]. RODRIGUES, C.A.D., “Titanium and molybdenum content in supermartensitic stainless steel.” Materials Science and Engineering A 460-461 (2007) 149-152.

[16]. SINDORIN, D., “The electrochemistry of 13% chromium stainless steel in oilfield brines.” Electrochimica Acta 50 (2005) 4109-4116.

[17]. SOUZA, E. C., “Influence of chloride ion concentration and temperature on the electrochemical properties of passive films formed on a superduplex stainless steel.” Materials Characterization 61 (2010) 240-244, São Paulo.

[18]. YANLIANG, H., “Sensitisation identification of stainless steel to intergranular stress corrosion cracking by atomic force microscopy.” Materials Letters 62 (2008) 1863-1866, China.

[19]. YIN, Z. F., “Pitting behavior on super 13Cr stainless steel in 3,5% NaCl solution in the presence of acetic acid.” J Solid State Eletrochem (2009) 13:1291-1293, China.

Table 1 - Chemical composition of samples of steel 13Cr and S13Cr

	Elements														
Sample	C	Si	Mn	P	S	Cu	Al	Cr	Mo	Ni	V	Ti	Nb	Co	W	Fe
1-S13Cr	0	0,248	0,393	0,007	0	0,195	0,048	12,11	2,025	5,8	0,049	0,088	0,024	0,027	0,095	78,9
2-S13Cr	0,008	0,238	0,394	0,018	0	0,055	0,02	13,3	2,186	5,55	0,022	0,002	0,018	0,045	0,072	78,07
3-13Cr	0,178	0,122	0,435	0,01	0	0,018	0,015	13,28	0,032	0,14	0,02	0	0,004	0,001	0,017	85,72
4-13Cr	0,188	0,287	0,447	0	0	0,174	0,077	12,65	0,047	0,2	0,019	0,001	0,007	0,003	0,029	85,88

Table 6 - Table of equations for computing the nickel equivalent and chromium equivalent.

Nickel equivalent, is given by:
% Ni + 0,5 % Mn + 30% C
Chromium equivalent is given by:
% Cr + % Mo + 1.5% Si + 0.5% Nb + 2% Ti

Table 7 - Results of nickel equivalent

	Ni Equiv.	Ni	0,5*Mn	30*C
1-S13Cr	5,9965	5,8	0,393	0
2-S13Cr	5,987	5,55	0,394	0,008
3-13Cr	5,6975	0,14	0,435	0,178
4-13Cr	6,0635	0,2	0,447	0,188

Table 8 - Results of chromium equivalent

	Cr Equiv.	Cr	Mo	1,5*Si	0,5*Nb	2*Ti
1-S13Cr	14,695	12,11	2,025	0,248	0,024	0,088
2-S13Cr	15,896	13,3	2,186	0,238	0,018	0,022
3-13Cr	13,497	13,28	0,032	0,122	0,004	0
4-13Cr	13,133	12,65	0,047	0,287	0,007	0,001

Table 9 - Results of Anodic polarization curves, current (A) 50 to 100 mV above the corrosion potential, pitting pontecial domain passivity - 5% NaCl

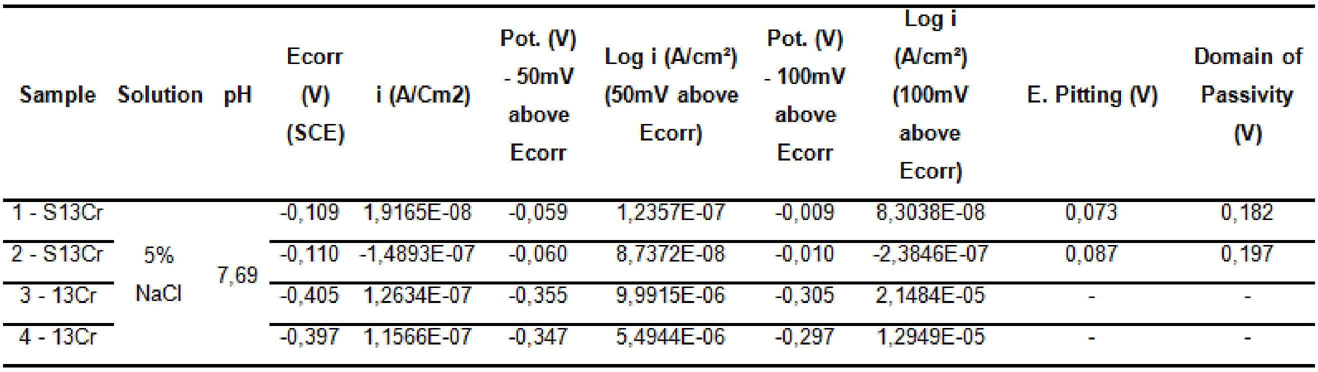

Sample	Solution	pH	Ecorr (V) (SCE)	i (A/Cm2)	Pot. (V) - 50mV above Ecorr	Log i (A/cm²) (50mV above Ecorr)	Pot. (V) - 100mV above Ecorr	Log i (A/cm²) (100mV above Ecorr)	E. Pitting (V)	Domain of Passivity (V)
1 - S13Cr	5% NaCl	7,69	-0,109	1,9165E-08	-0,059	1,2357E-07	-0,009	8,3038E-08	0,073	0,182
2 - S13Cr			-0,110	-1,4893E-07	-0,060	8,7372E-08	-0,010	-2,3846E-07	0,087	0,197
3 - 13Cr			-0,405	1,2634E-07	-0,355	9,9915E-06	-0,305	2,1484E-05	-	-
4 - 13Cr			-0,397	1,1566E-07	-0,347	5,4944E-06	-0,297	1,2949E-05	-	-

Table 10 - Results of Anodic polarization curves, current (A) 50 to 100 mV above the corrosion potential, pitting pontecial domain passivity - 10% NaCl

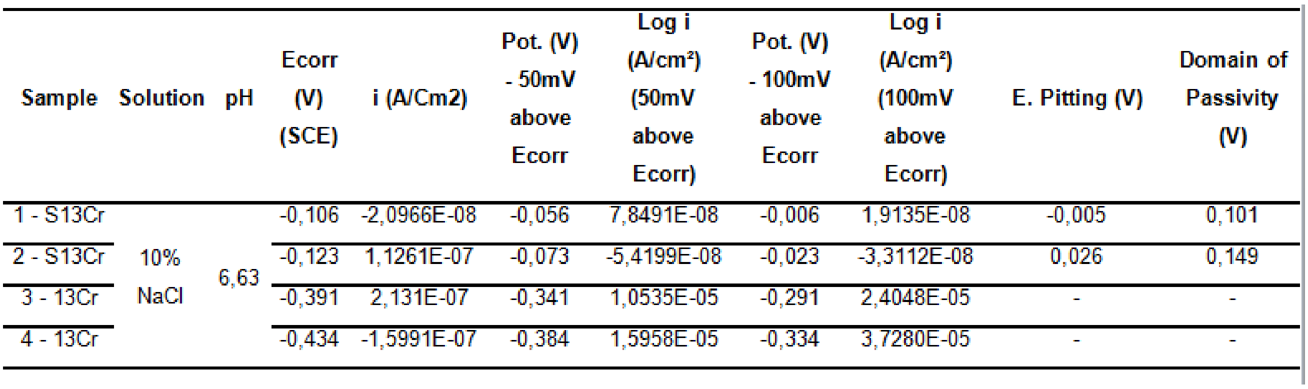

Sample	Solution	pH	Ecorr (V) (SCE)	i (A/Cm2)	Pot. (V) - 50mV above Ecorr	Log i (A/cm²) (50mV above Ecorr)	Pot. (V) - 100mV above Ecorr	Log i (A/cm²) (100mV above Ecorr)	E. Pitting (V)	Domain of Passivity (V)
1 - S13Cr	10% NaCl	6,63	-0,106	-2,0966E-08	-0,056	7,8491E-08	-0,006	1,9135E-08	-0,005	0,101
2 - S13Cr			-0,123	1,1261E-07	-0,073	-5,4199E-08	-0,023	-3,3112E-08	0,026	0,149
3 - 13Cr			-0,391	2,131E-07	-0,341	1,0535E-05	-0,291	2,4048E-05	-	-
4 - 13Cr			-0,434	-1,5991E-07	-0,384	1,5958E-05	-0,334	3,7280E-05	-	-

Table 11 - Results of Anodic polarization curves, current (A) 50 to 100 mV above the corrosion potential, pitting pontecial domain passivity - 20% NaCl

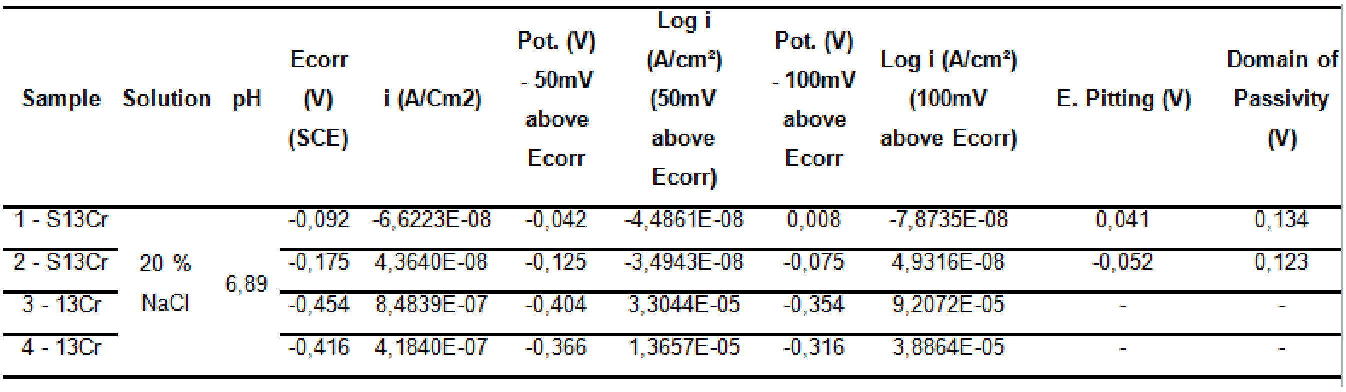

Sample	Solution	pH	Ecorr (V) (SCE)	i (A/Cm2)	Pot. (V) - 50mV above Ecorr	Log i (A/cm²) (50mV above Ecorr)	Pot. (V) - 100mV above Ecorr	Log i (A/cm²) (100mV above Ecorr)	E. Pitting (V)	Domain of Passivity (V)
1 - S13Cr	20 % NaCl	6,89	-0,092	-6,6223E-08	-0,042	-4,4861E-08	0,008	-7,8735E-08	0,041	0,134
2 - S13Cr			-0,175	4,3640E-08	-0,125	-3,4943E-08	-0,075	4,9316E-08	-0,052	0,123
3 - 13Cr			-0,454	8,4839E-07	-0,404	3,3044E-05	-0,354	9,2072E-05	-	-
4 - 13Cr			-0,416	4,1840E-07	-0,366	1,3657E-05	-0,316	3,8864E-05	-	-

Table 12 – Impedance, Real Polarization Resistance

Super Martensitic Steel			**Martensitic Steel**		
Pontential	**Real Resistence (Ω)**		**Pontential**	**Real Resistence (Ω)**	
	Sample 1	**Sample 2**		**Sample 3**	**Sample 4**
On OCP	247740	259860	On OCP	11670	10168
50mV above OCP	248570	275430	50mV above OCP	12475	7114,8
150 mV above OCP	323190	334130	100 mV above OCP	11669	2788,8

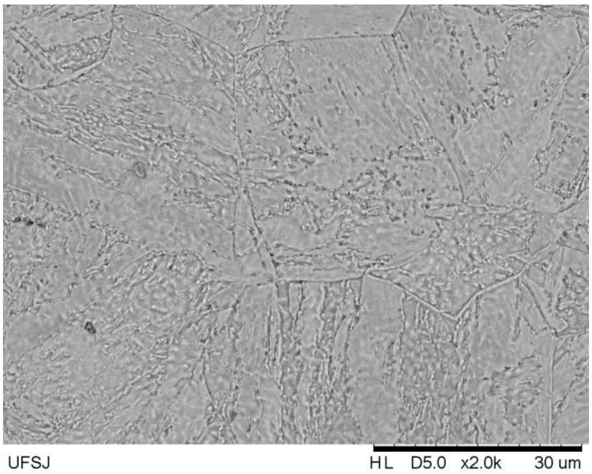

Figure 2. Microstructure of steel 1-S13Cr (SEM), X2000 Vilella chemical attack.

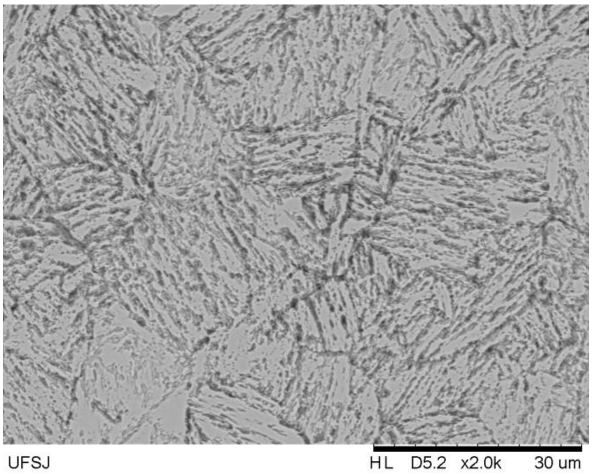

Figure 3. Microstructure of steel 2-S13Cr(SEM), X2000 Vilella chemical attack.

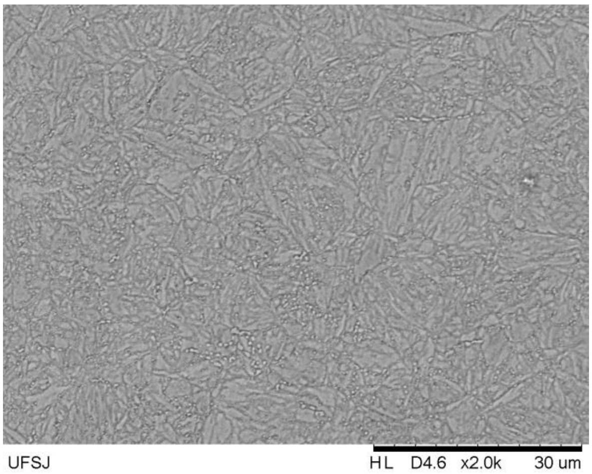

Figure 4. Microstructure of steel 3-13Cr (SEM), X2000 Vilella chemical attack.

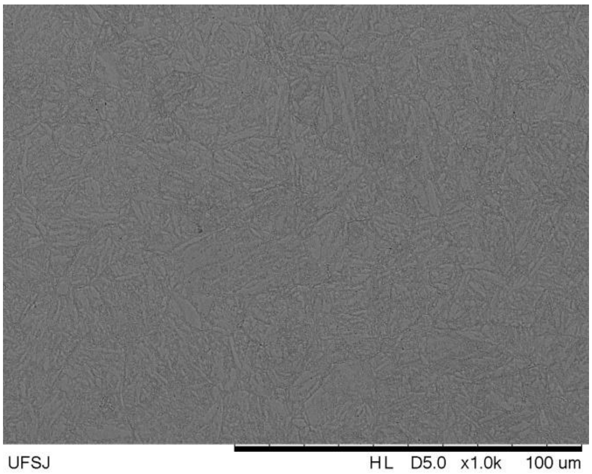

Figure 5. Microstructure of steel 4-13Cr (SEM), X1000 Vilella chemical attack.

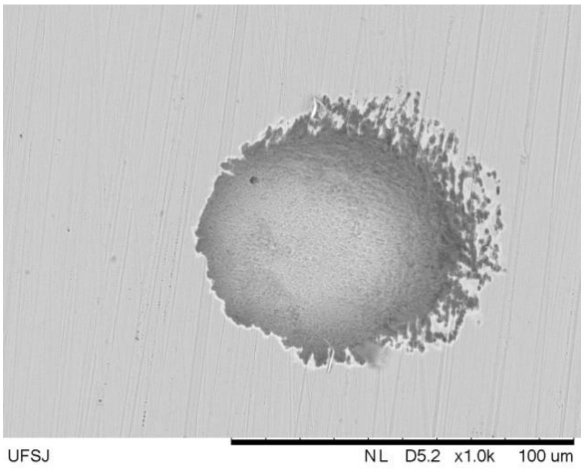

Figure 6. Microstructure of steel 1-S13Cr (SEM), X1000

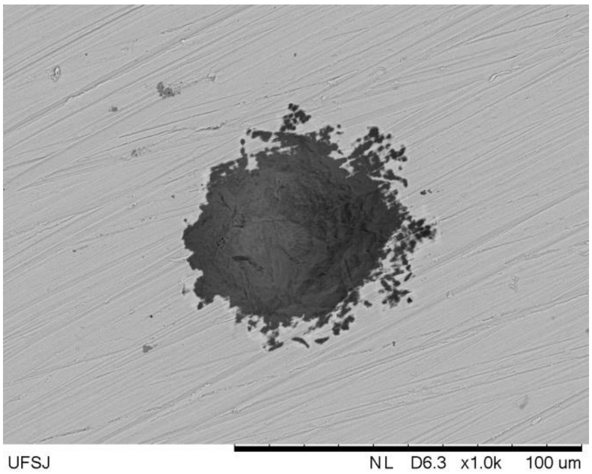

Figure 7. Microstructure of steel 2-S13Cr (SEM), X1000

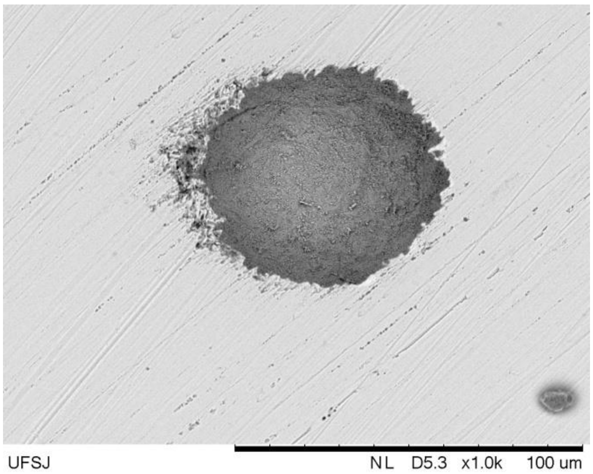

Figure 8. Microstructure of steel 3-13Cr (SEM), X1000

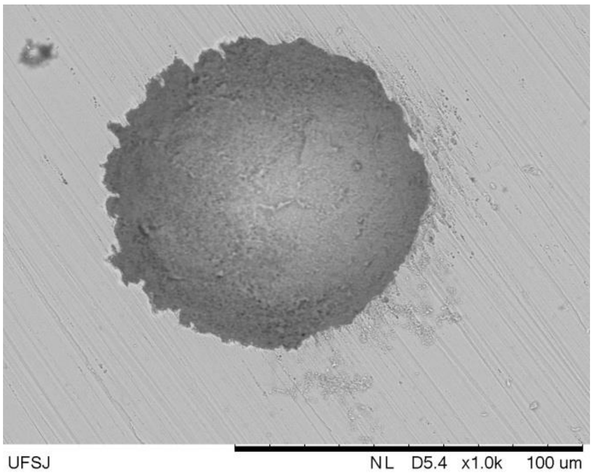

Figure 9. Microstructure of steel 4-13Cr (SEM), X1000

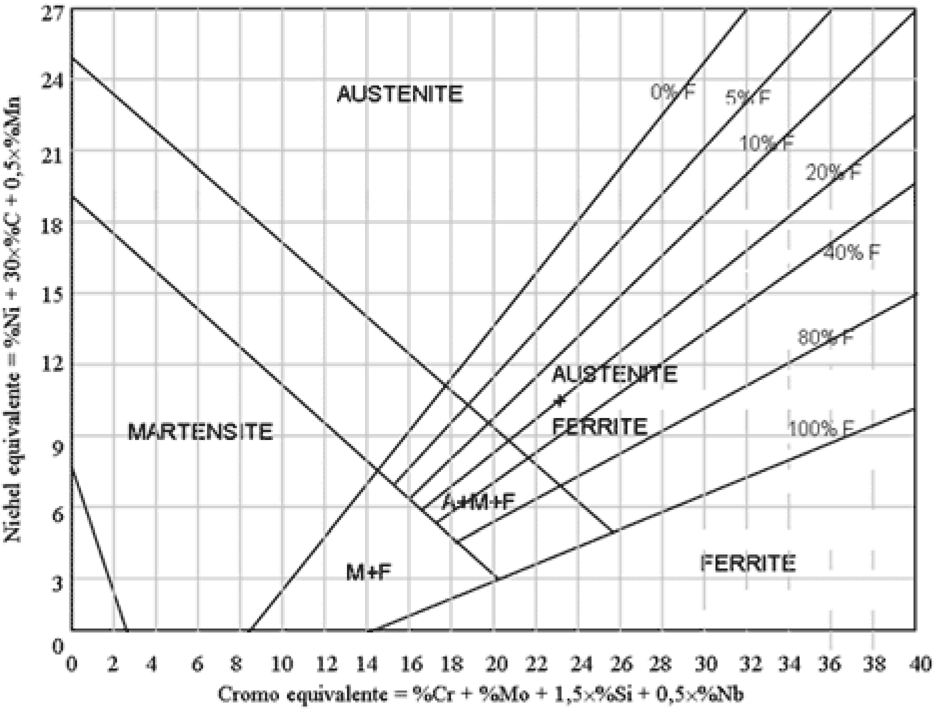

Figure 10 – Scheaffler diagram

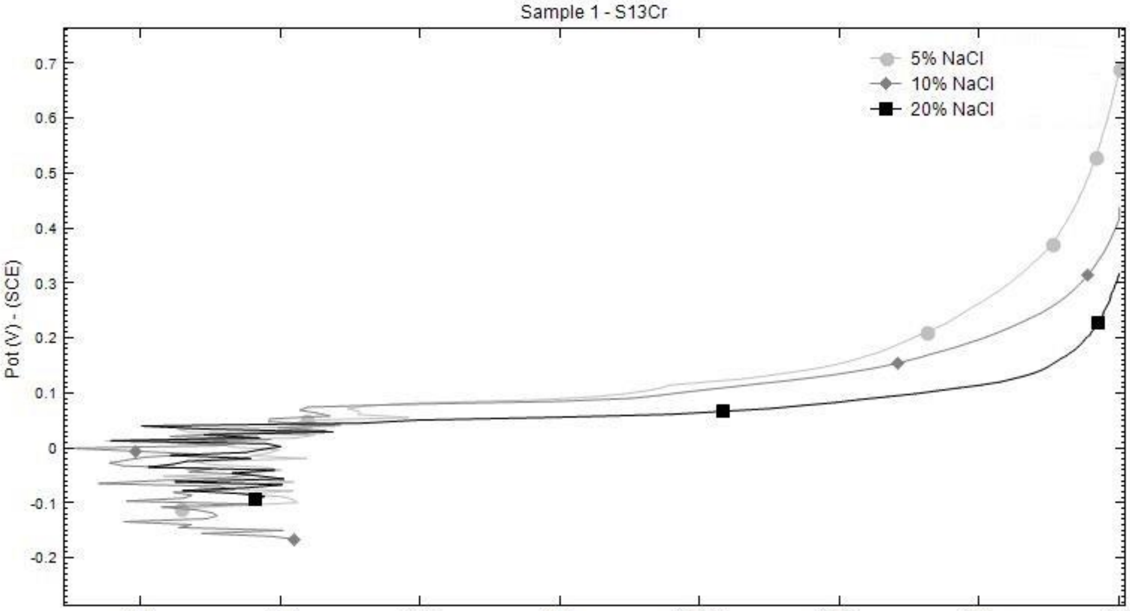

Figure 11 - Polarization Curves – Sample 1

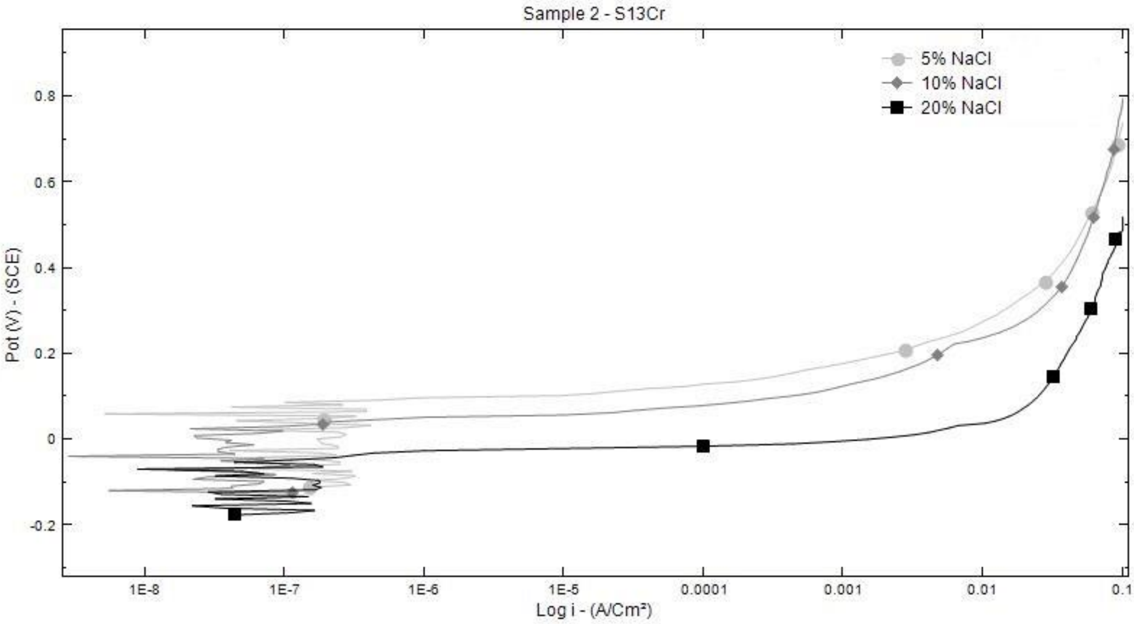

Figure 12 - Polarization Curves – Sample 2

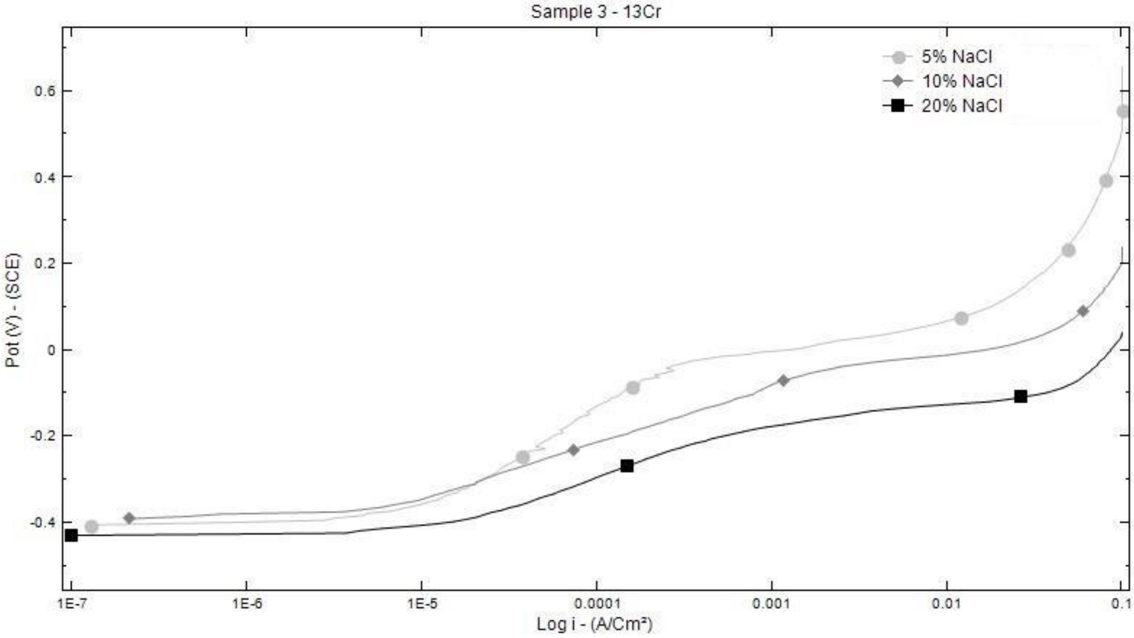

Figure 13 - Polarization Curves – Sample 3

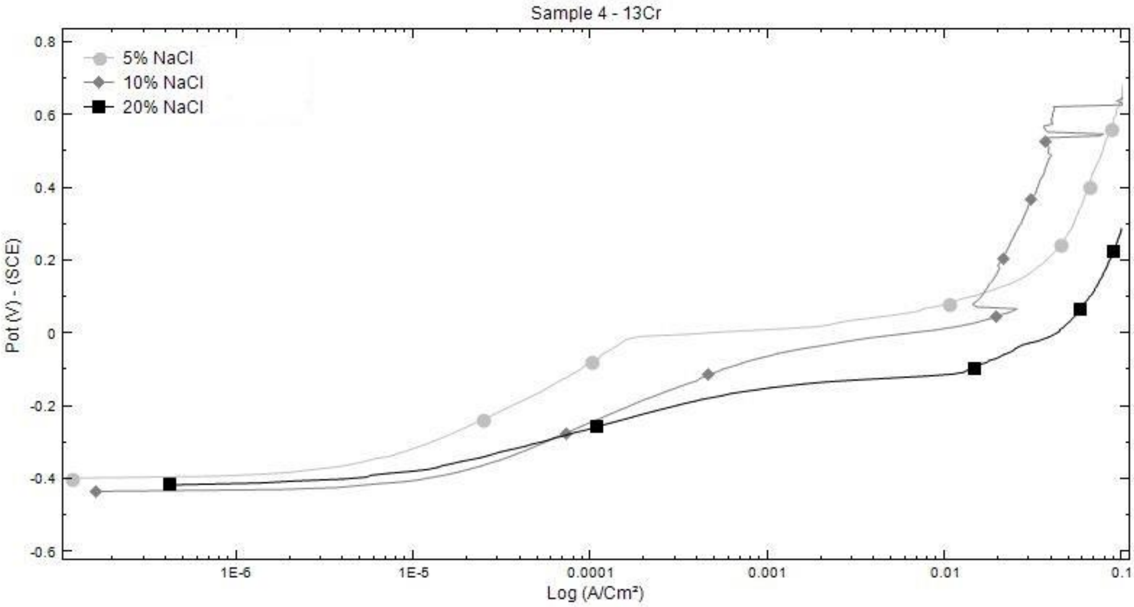

Figure 14 - Polarization Curves – Sample 4

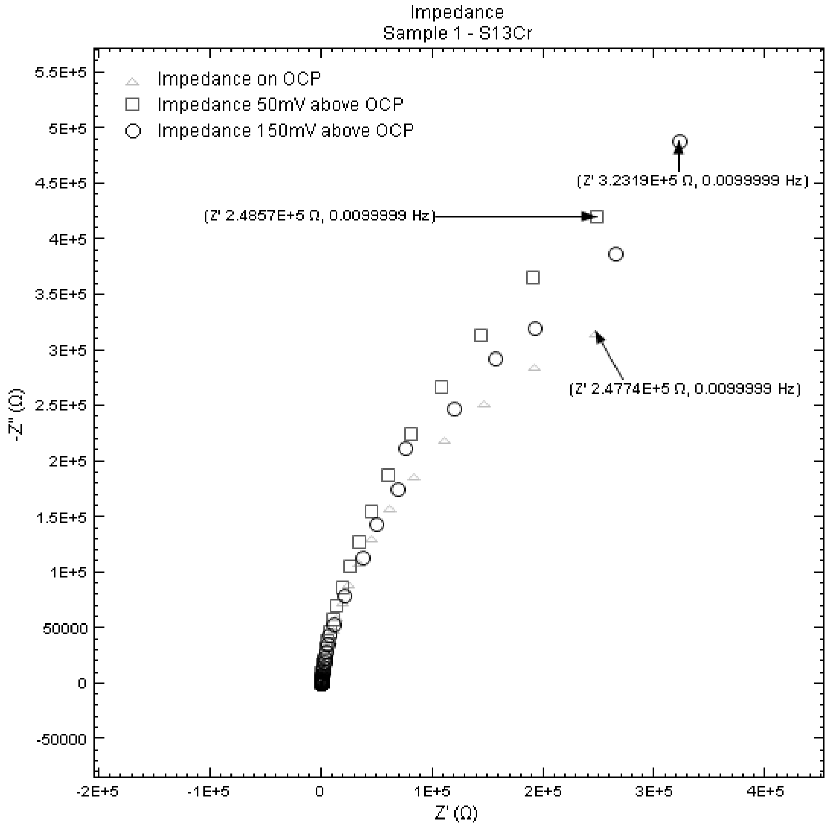

Figure 15 – Nyquist Impedance Curve for Super martensitic stainless steel in 5% NaCl Solution – Sample 1

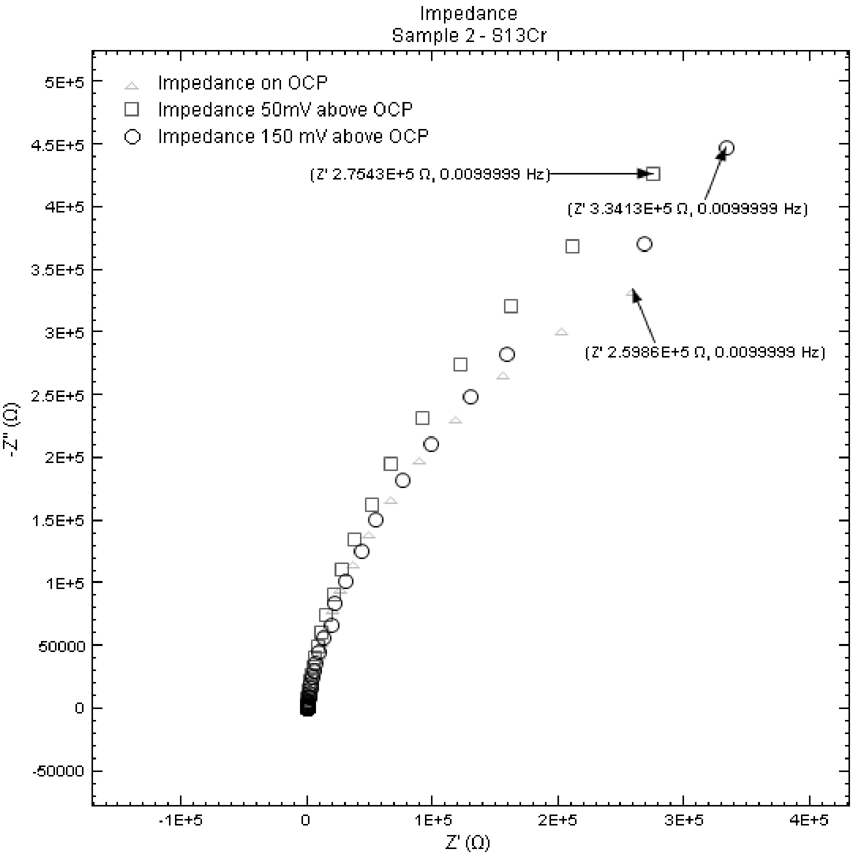

Figure 16- Nyquist Impedance Curve for Super martensitic stainless steel in 5% NaCl Solution – Sample 2

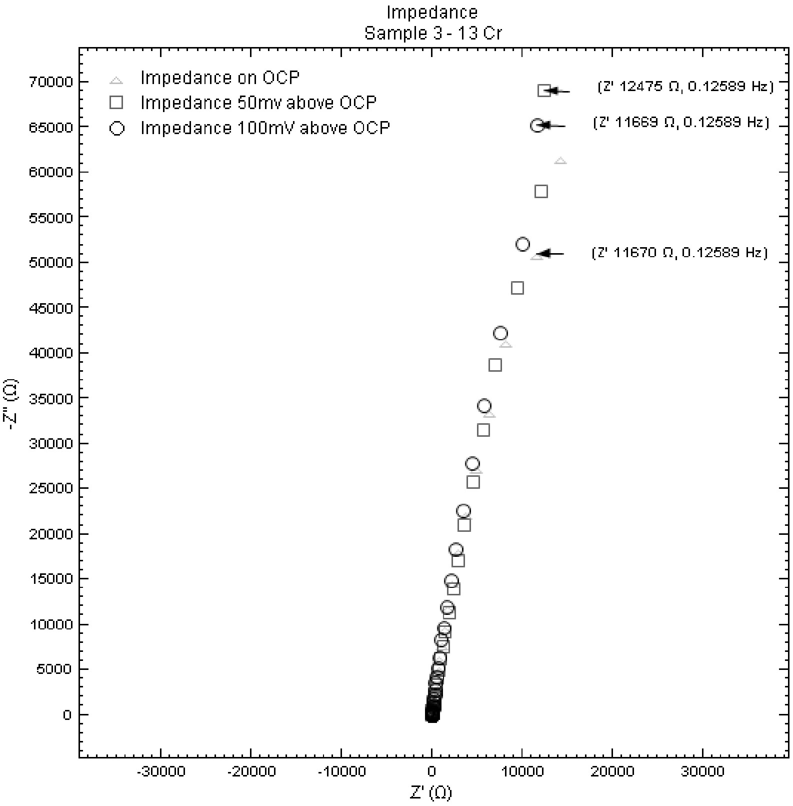

Figure 17– Nyquist Impedance Curve for Martensitic stainless steel in 5% NaCl Solution – Sample 3

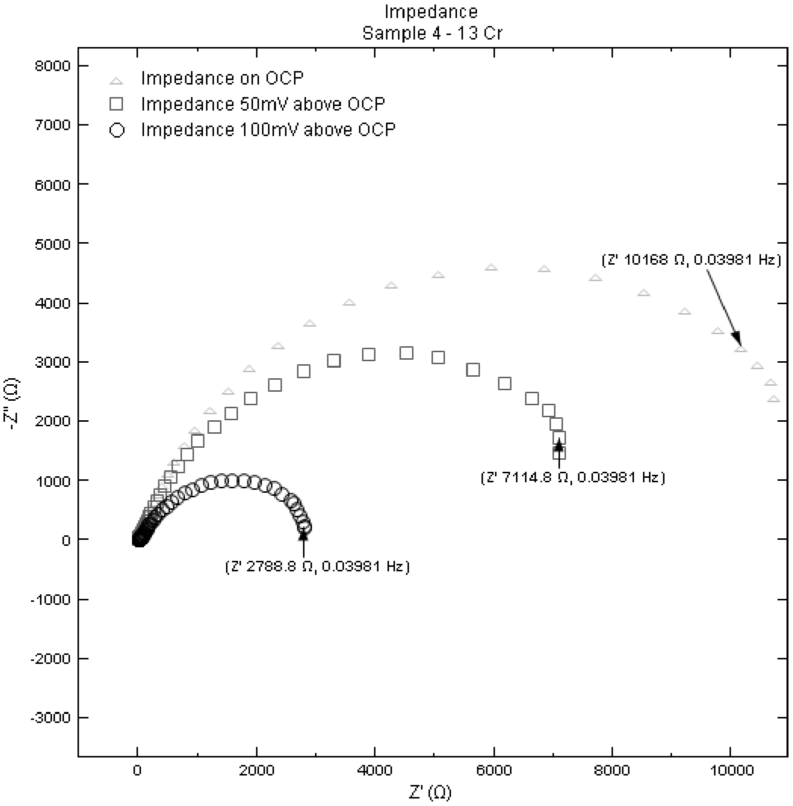

Figure 18– Nyquist Impedance Curve for Martensitic stainless steel in 5% NaCl Solution – Sample 4

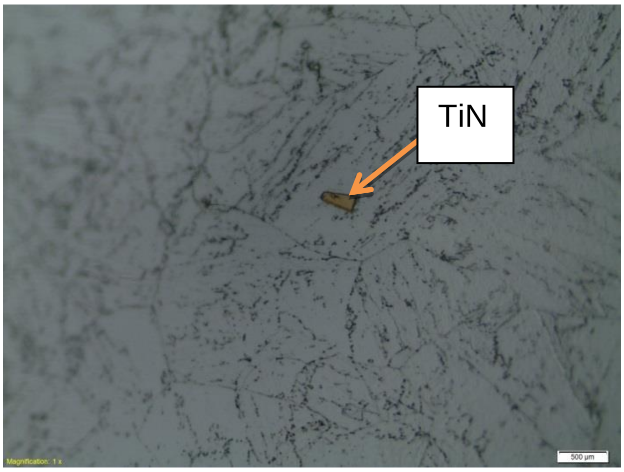

Figure 19 - A – MO identificação de precipitados de Ti – Sample 1

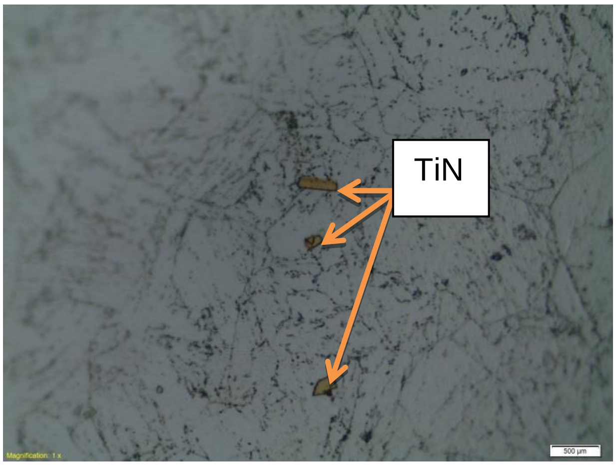

Figure 19 - B – MO, identificação de precipitados de Ti – Sample 1

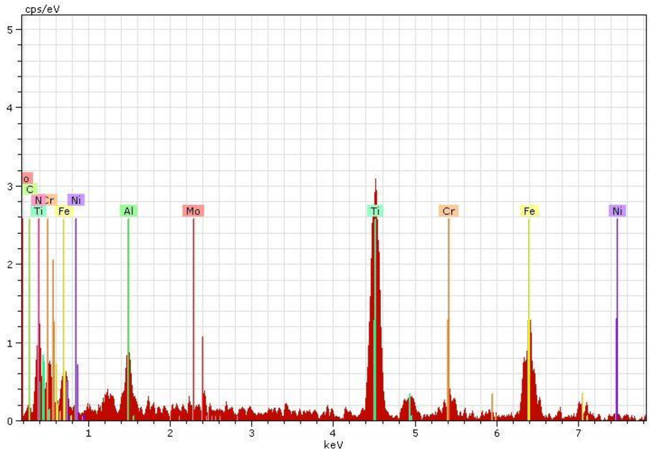

Figure 20-A - EDS analyses TiN

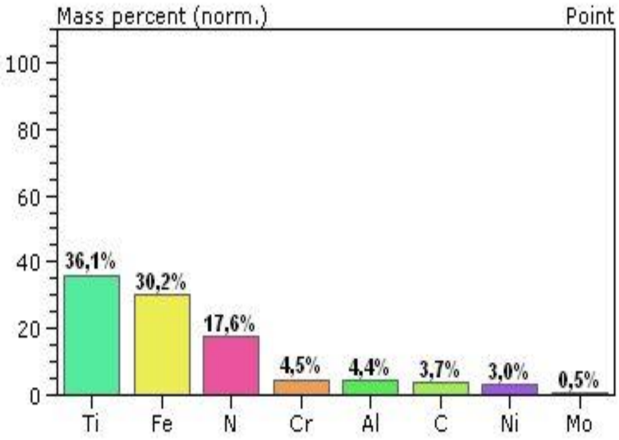

Figure 20-B EDS analyses TiN

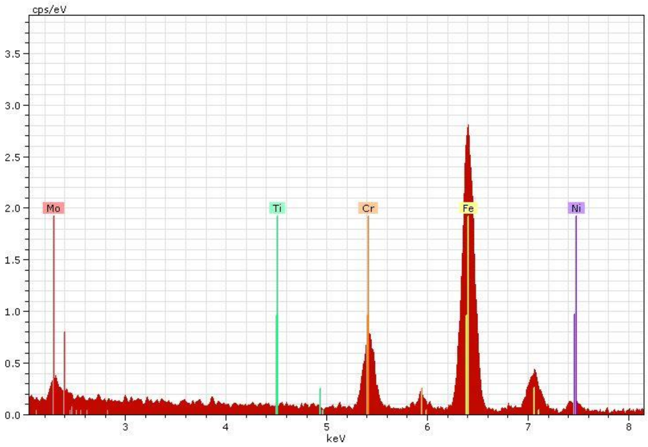

Figure 21-A - EDS analyses

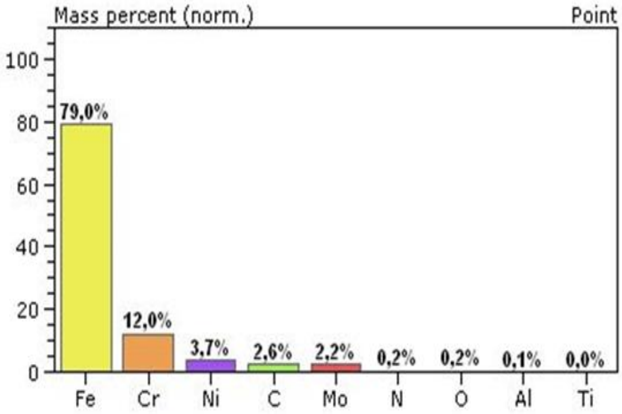

Figure 21 - B – EDS analyses